Combining Bioinspired Red Kite Optimization and Deep Learning for Effective COVID-19 Detection in Chest Radiography

Mohammed Altaf Ahmed[1,*], Suleman Alnatheer[1], Sachi Nandan Mohanty[2], Paruchuri Pavan Kumar[3], Bibhuti Bhushan Dash[4], and Qutubuddin Mohammed[5]

[1]Department of Computer Engineering, College of Computer Engineering and Sciences, Prince Sattam bin Abdulaziz University, Al-Kharj, Saudi Arabia
[2]School of Computer Science & Engineering (SCOPE), VIT-AP University, Amaravati, Andhra Pradesh, India
[3]Department of Artificial Intelligence and Data Science, Faculty of Science and Technology (ICFAITECH), ICFAI Foundation for Higher Education, Hyderabad, India
[4]School of Computer Applications, KIIT Deemed to be Univsity, Bhuabneswar, Odisha, India
[5]Department of Electrical Engineering, College of Engineering Wadi Addawasir, Prince Sattam bin Abdulaziz University, Saudi Arabia
Email: m.altaf@psau.edu.sa (M.A.A.); s.alnatheer@psau.edu.sa (S.A.); sachinandan09@gmail.com (S.N.M.); pavanpk@ifheindia.org (P.P.K.); bibhuti.dash@gmail.com (B.B.D.); q.mohammed@psau.edu.sa (Q.M.)
[*]Corresponding author

Manuscript received June 14, 2025; revised July 24, 2025; accepted November 25, 2025; published March 31, 2026

***Abstract*—Deep Learning (DL)-based systems, employing advanced growths, pave the way for bioinspired methods in almost all domains of life. Healthcare organizations can employ DL approaches due to their precision in recognizing and identifying distinct diseases. The coronavirus disease (COVID-19) epidemic has emerged as the most dangerous disease in recent times, posing a significant burden on health organizations worldwide. Medical imaging and PCR testing have the potential to analyze COVID-19. Given the high spreadability of COVID-19, Chest X-Ray (CXR) analysis is considered safe under various conditions. DL systems are capable of enhancing medical imaging tools and supporting radiologists in making medical decisions for the analysis, diagnosis, and monitoring of distinct diseases. With this motivation, this study presents a novel bioinspired red kite optimizer with a DL-based COVID-19 classification (BRKODL-COVIDC) method on CXR images. The BRKODL-COVIDC method intends to recognize and categorize the presence of COVID-19 using DL models. In the presented BRKODL-COVIDC method, the Bilateral Filtering (BF) model can be used for image pre-processing tasks. In addition, the complex patterns and features in the images can be derived from the DenseNet121 model. For optimal hyperparameter selection of the DL techniques, the Random Key Optimizer (RKO) model can be employed in this research. Last, the BRKODL-COVIDC technique makes use of the Dilated Convolutional Auto-Encoder (DCAE) model and is used for identification purposes. Thus, with this research study, we are contributing to the National Priorities for Research, Development, and Innovation (RDI) in health and wellness to provide and maintain a sustainable environment in the health sector. The simulation outputs of the BRKODL-COVIDC technique can be examined on a standard dataset. The simulated outputs demonstrated the enhanced performance of the BRKODL-COVIDC technique in the COVID-19 detection procedure.**

***Keywords*—computer-aided diagnosis, bioinspired algorithms, deep learning, intelligent systems, leukaemia cancer, sustainable environment, healthcare**

I. Introduction

COVID-19 is the latest viral epidemic, which began in Wuhan City in China. It spreads to every part of the world within a few months. It is an extremely transmittable disease that spreads through respiring droplets while breathing [1]. For testing COVID-19 cases, imaging models, namely Computed Tomography (CT) and X-ray, play a significant part [2]. As the disease commonly infects the lungs, chest radiography images (CT images or CXR) become broadly measured, and radiologists physically do the analysis of these images to detect pictorial signs of COVID-19 disease [3]. For quick checking for the diseased patient, visual indicators can serve as an alternate technique. The conservative analysis method is comparatively rapid but still creates a higher threat for medicinal staff [4]. There are limited analytical tests since they are expensive. In contrast, medical imaging methods, namely CT and X-ray screening, are faster, safer, and readily available. X-ray imaging has been widely utilized in COVID-19 check-ups, as it involves fewer imaging periods, the charge is also lower, and X-ray scanners are broadly accessible in rural sectors compared to CT imaging [5]. However, the visual assessment of X-ray images by radiologists at a large scale is long and weighty and can result in wrong analysis because of the absence of prior awareness about the infected areas. Therefore, there is a great requirement for designing mechanized approaches to get effective COVID-19 analysis [6, 7].

To save effort and time, it is significant to mechanize the CXR inquiry, which is an extensive and errant method that consumes effort and time [8, 9]. Consequently, fully mechanized and actual radiography images are essential to help physicians precisely identify the COVID-19 virus. Doctors can use Computer Added Design (CAD) methods that rely on DL approaches to help them understand and analyze CXR images better and to overcome the challenges of current imaging techniques. DL approaches are frequently used in medical imaging because they can handle large datasets that surpass human capabilities. Uniting CAD methods with radiologists' medical diagnostics reduces doctors' pressure and develops precision and arithmetical inquiry. The modern mechanized approaches employ modern-day Artificial Intelligence (AI) tools (mostly the DL method) to develop the control of CXR imaging and are

meant to diminish the work of radiologists [10, 11]. DL methods, particularly Convolution Neural Network (CNN), have been shown to be more efficient than outdated AI approaches and are broadly utilized for studying numerous medical images [12, 13].

This study presents a novel bioinspired red kite optimizer with a DL-based COVID-19 classification (BRKODL-COVIDC) method on CXR images. The BRKODL-COVIDC method intends to recognize and categorize the presence of COVID-19 using DL models. In the presented BRKODL-COVIDC method, the Bilateral Filtering (BF) model can be used for image pre-processing tasks. In addition, the complex patterns and features in the images can be derived from the DenseNet121 model. For optimal hyperparameter selection of the DL techniques, the RKO model can be employed in this research. Last, the BRKODL-COVIDC technique makes use of the Dilated Convolutional Auto-Encoder (DCAE) model and is used for identification purposes. The simulation outputs of the BRKODL-COVIDC technique can be examined on a standard dataset. This research aims to target study, development, and innovation in health and wellness and contribute to providing a sustainable health environment.

II. Literature Review

Gupta and Bajaj [14] present a model utilizing the DL and chest CT scan-related methods. In this article, an openly available CT-scan image dataset, a couple of pre-trained DL methods (DLMs), viz., MobileNetV2 and DarkNet19, and an innovatively developed frivolous DLM could be used for automated screening of COVID-19. A recurring 10-fold holdout authentication technique is used for the testing, validation, and training of DLMs. Mansour *et al.* [15] presented an innovative unsupervised DL-based Unsupervised Deep Learning based Variational Auto Encoder (UDL VAE) system. The UDL-VAE method elaborates an Adaptive Wiener Filtering (AWF) assisted preprocessing method to improve image excellence. In Refs. [16,17], a feasible and effective DL-based Chest Radiograph Classification (DL-CRC) structure is proposed. This structure controls a Data Augmentation of Radiograph Images (DARI) approach by adaptably using generic data augmentation and Generative Adversarial Network (GAN) approaches. The training information consists of real and artificial CXR images that were served and modified as the CNN method in DL-CRC.

Subhalakshmi *et al.* [18] and Shankar *et al.* [19] proposed a DL-based MultiModal Fusion (DLMMF) method. This method works in three key procedures, viz., WF is dependent upon feature extraction, preprocessing, and identification. The projected method integrates a combination of deep features utilizing the Inception v4 and VGG16 methods. Lastly, the Gaussian Naïve Bayes (GNB) method has been presented for recognizing and classifying CT images into separate classes. Shanthi and Koppu [20] and Dash *et al.* [21] presented effective methods named RNBO_Deep Neuro-Fuzzy Network (RNBO_DNFN) and Remora Namib Beetle Optimizer_Deep Quantum-NN (RNBO_DQNN) method. This method has been aimed at integrating Namib Beetle Optimization (NBO) and the Remora Optimization Algorithm (ROA) to improve performance. In two other studies [22, 23], a new IoT-allowed depthwise separable CNN (DWS-CNN) with the Deep-SVM (DSVM) method is proposed. Primarily, patient information is composed by utilizing IoT devices and directed towards the cloud server. Also, the GF method was used for noise elimination. Then, the DWS-CNN method is used for automatically extracting features. Lastly, the DSVM method could be used to control the multiple and binary classes of COVID-19.

Sharma *et al.* [24] proposed 16 deep learning-based systems for segmentation and identification. They used two segmentation networks (UNet and UNet+) along with eight classification models: VGG19, VGG16, InceptionV3, Xception, NASNetMobile, ResNet50, MobileNet, and DenseNet201. The performance of these systems was evaluated using Jaccard, Dice, Area Under the Curve (AUC), and Receiver Operating Characteristics (ROC) metrics, and explainability was provided through Gradient-weighted Class Activation Mapping (Grad-CAM).

In another study [25], a method called Sine-Cosine Optimization + DL-based Disease Detection and Classification (SCODL-DDC) was introduced, which combines a sine cosine optimizer with deep learning. EfficientNet was used to extract features, and the Sine Cosine Optimizer (SCO) tuned the model parameters. A Quantum Neural Network (QNN) was also applied for accurate COVID-19 detection.

III. Materials and Methods

In this paper, a programmed COVID-19 identification and classification algorithm, named BRKODL-COVIDC technique on CXR images, is proposed. The BRKODL-COVIDC method intends to recognize and categorize the existence of COVID19 employing DL models. In this developed BRKODL-COVIDC approach, four main processes such as BF-based pre-processing, RKO based hyperparameter tuning, DenseNet121 feature extractor, and DCAE based classification. Fig. 1 represents the workflow of BRKODL-COVIDC method.

A. Image Pre-processing Using BF Approach

For noise elimination, the BF approach is utilized. BF is an image processing system utilized to smooth noise reduction while maintaining boundaries from the image [26]. A nonlinear, edge-preserving filter integrates spatial domain and intensity (pixel value) domain data to achieve its effects. BF is mainly effective in conditions, but typical smoothing filters can blur edges and fine details. The basic concept behind BF is to execute a weighted average for the pixel values from the local neighborhood but assuming either spatial closeness or intensity similarity. The weight of all the pixels is defined by the Gaussian function in either the spatial or the intensity domains. The working of BF is provided as follows:

Spatial Domain: A window (kernel) is determined near all the pixels from the image. This window defines the spatial neighborhood for which filtering can be executed.

Intensity Domain: During the spatial window, the pixel values can be related depending on their intensities. A Gaussian kernel can be executed for computing the weighted dependence upon intensity similarity. Pixels with the same intensity values are superior weights, meaning they

contribute more to the filtered outcome.

Weighted Average: For all the pixels from the image, the weighted average of pixel values from the spatial window can be calculated. The weights are defined by either spatial closeness or intensity similarity.

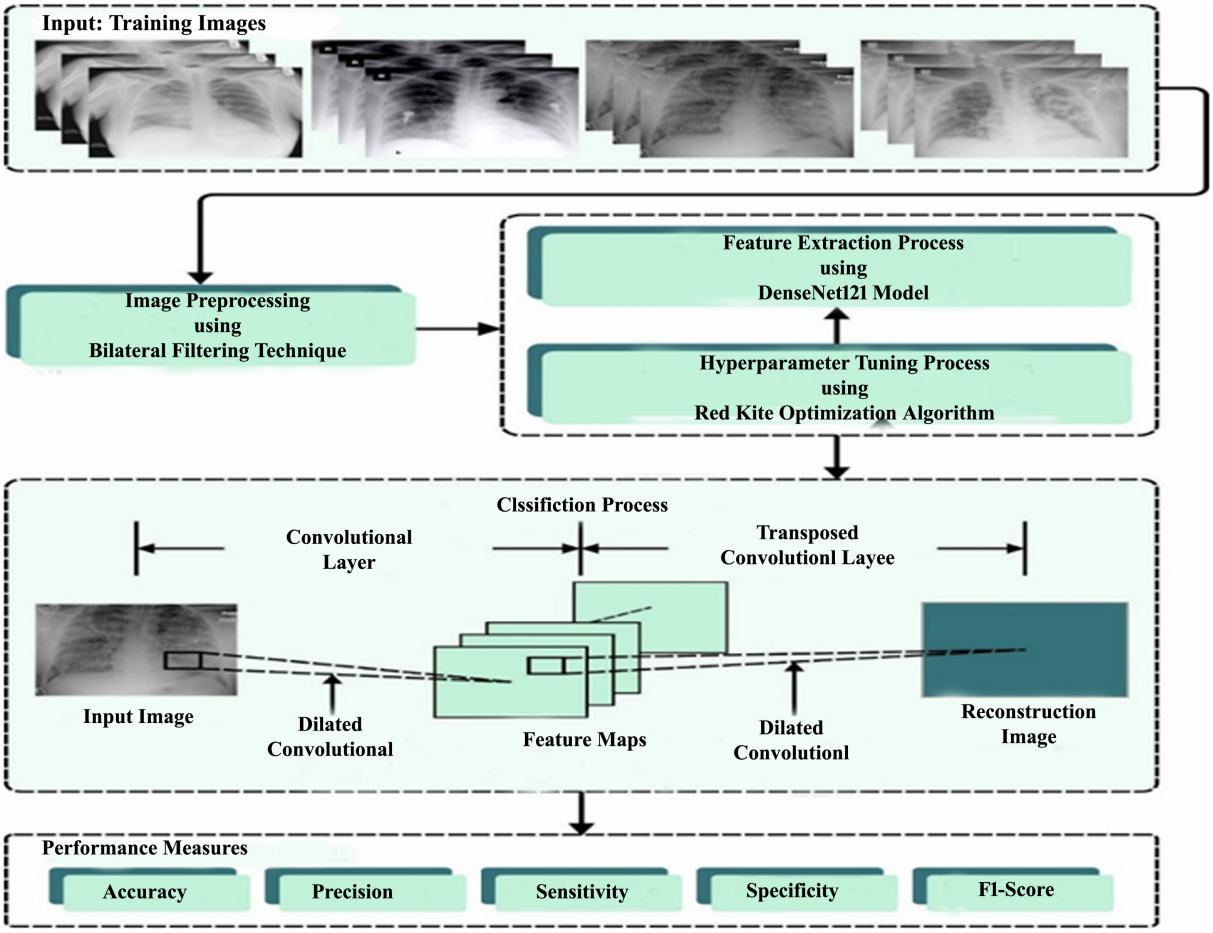

Fig. 1. Workflow of BRKODL-COVIDC approach.

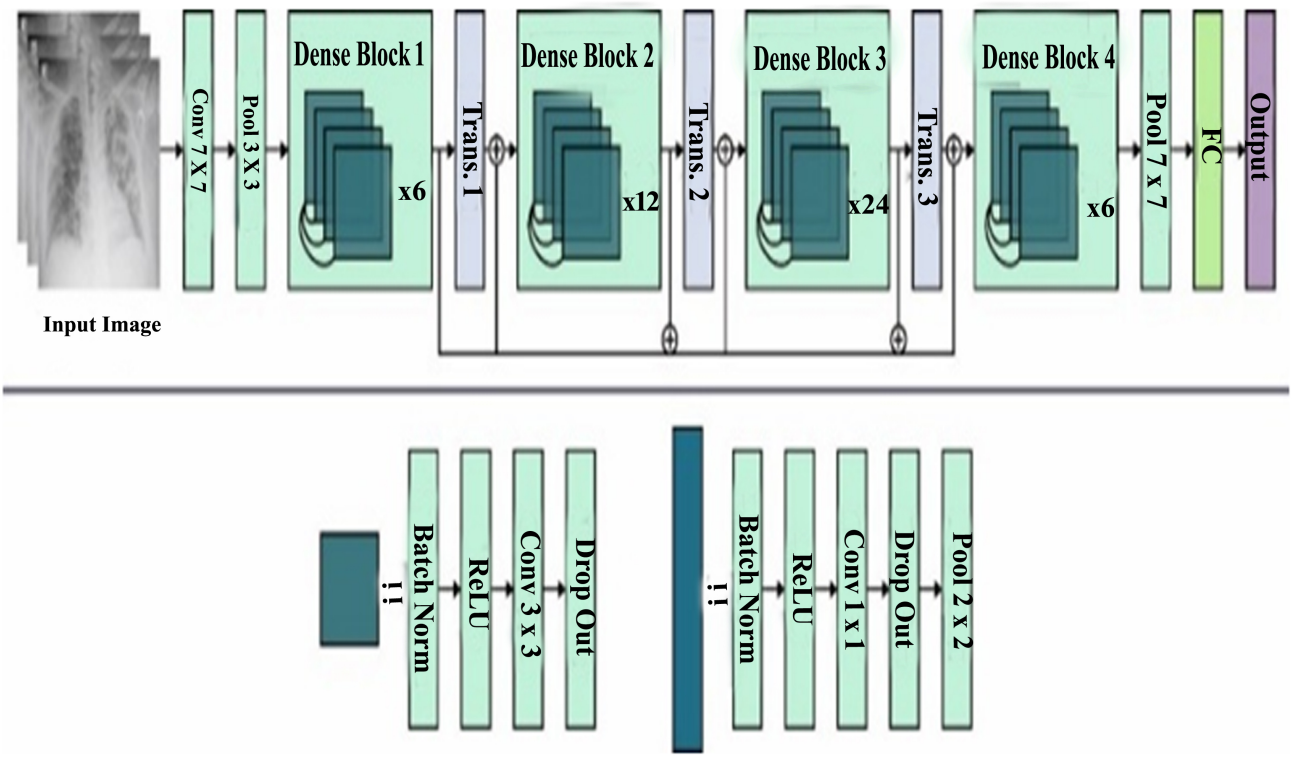

Fig. 2. DenseNet structure.

B. DenseNet121-Based Feature Extraction

For generating beneficial feature sets, the DenseNet121 framework is applied. DenseNet features a network model that focuses on developing Deep Learning (DL) systems while also enhancing training efficiency by utilizing smaller connections between layers [27]. All the layers get upgraded inputs among every future level, and it is done for the feature space to every next layer for maintaining the feed-forward nature. The process of removing features from the data and mapping them to labels for categorization in a database resulted in the creation of a CNN approach. PyTorch and Torchvision (2 DL libraries) are also needed to finish this task. Torchvision is a pretraining data modeling system that offers a maximum level of mechanism beside overfitting and also improves the optimizer of outcomes. The number 121 in DenseNet121 represents that the NN takes 121 layers, which is an essential feature. The DenseNet-121 comprises several distinct layers to be integrated. The task of the DenseNet method consists of dense blocks and transition layers, which are utilized for categorizing an input evaluation based on its contents. When a text is input into the DenseNet, it can be processed using multiple dense blocks that map features from all the consistent layers, even though the number of filters varies from one layer to another within a single dense block. Convolution and pooling are two procedures managed by the transition layer. It is placed external to the dense layer and carries out down-sampling processes. Fig. 2 depicts the architecture of DenseNet.

C. Hyperparameter Tuning Utilizing RKO Model

In this manuscript, the RKO model optimizes the hyperparameter values of the DenseNet121 framework. Alshareef and Fathy [28] introduced the Red Kite Optimizer Algorithm (ROA), a new metaheuristic algorithm based on the social life of red kites.

Typically, the red kite constructs nests near lakes and wooded areas to enhance their hunting capabilities. With random walking and being impacted by one another's locations in flight, they use high speed while hunting. It can be a voiced, named sound of unity that occurs in times such as identifying water sources, useful bait, birth, and migration. Additionally, the sound generated during events such as the death of another animal, an enemy attack, a storm, or an earthquake is called the sound of danger. To emulate the behaviors of a red kite in search of food, every individual bird is determined by the evaluation function value, its position, the individual component (sound of danger), the amount of displacement of points, the new location of the bird, the new assessment function, and the social component (sound of unity). Firstly, the metaheuristic approach must effectively navigate the search space problem to prevent stumbling into local optima, thereby achieving superior outcomes. Next, the approach gradually transitions from the exploration stage to the exploitation stage while also exploiting the fittest solutions in the final round. The three major phases of ROA can be discussed below:

The initial phase—the initial location of the bird: the location of red kites is randomly initialized based on Eq. (1):

$$Pos_{i,j}(t) = lb + rand \times (ub - lb), i = 1,2,\dots,n \text{ and } j = 1,2,\dots,d \quad (1)$$

Now, $Pos_{i,j}(t)$ refers to i^{th} location of red kites at t iteration, lb, and ub are lower and upper limitations, respectively, d denotes the problem dimension, n is the population size, and $rand$ is a randomly produced value within [0, 1].

The second phase—choose the leader: according to Eq. (2) selecting the leader is attained:

$$\overrightarrow{Best(t)} = \overrightarrow{Pos_i(t)} \; if \; f_i(t) < f_{best}(t) \quad (2)$$

where, $Best(t)$ indicates the location of best bird at t^{th} iterations, $f_{besi}(t)$ can be the value of the assessment performance of the optimum bird at t^{th} iterations $Pos(t)$ represents the location of i^{th} red kites at t iteration, $f_i(t)$ is the value of bird assessment function at t^{th} iterations.

The third phase—the movement of the bird: by considering the decreasing coefficient (D), the red kite should move from the exploration to the exploitation phase based on Eq. (3):

$$D = \left(exp\left(\frac{t}{t\_max}\right) - \frac{t}{t\_max}\right)^{-10} \quad (3)$$

where t, and t_{max} denotes the existing and maximum iteration. By using Eqs. (4) and (5), the birds update the position:

$$\overrightarrow{pos_i^{new}(t+1)} = \overrightarrow{Pos_i(t)} + \overrightarrow{P_{mi}(t+1)} \quad (4)$$

$$\overrightarrow{P_{mi}(t+1)} = D(t) \times \overrightarrow{P_{mi}(t)} + \overrightarrow{SC(t)} \odot \left(\overrightarrow{Pos_{rws}(t)} - \overrightarrow{Pos_i(t)}\right) + \overrightarrow{UC(t)} \odot \left(\overrightarrow{Best(t)} - \overrightarrow{Pos_i(t)}\right) \quad (5)$$

As in Eq. (6), the birds location elected by the roulette wheel in iteration t as $Pos_{rws}(t)$, the new location of the bird as $pos_i^{new}(t+1)$, and the random vector of social and individual components are SC and UC, correspondingly. It is significant to test the search space-bound, as follows:

$$\overrightarrow{pos_i^{new}(t+1)} = \max\left(\min\left(\overrightarrow{pos_i^{new}(t+1)} + ub\right), lb\right) \quad (6)$$

If the assessment function is enhanced, then the new temporary location is replaced. In this instance, $Pos_i(t+1)$ is equal to $os_i^{new}(t+1)$. The sound of unity and danger of the bird as follows:

$$\begin{cases} \overrightarrow{SC(t+1)} = \overrightarrow{r_1} \\ \overrightarrow{UC(t+1)} = \overrightarrow{r_2} \end{cases} if \; rand \le 0.5$$

$$\begin{cases} \overrightarrow{SC(t+1)} = \overrightarrow{r_3} \\ \overrightarrow{UC(t+1)} = \overrightarrow{r_1} \end{cases} otherwise \quad (7)$$

In Eq. (7), $\overrightarrow{r_3}$ is a random vector in [0, 1]. $\overrightarrow{r_1}$ and $\overrightarrow{r_2}$ denotes a random vector in [1,2] and [1,3], respectively.

The location of the neighbor could be chosen randomly via the roulette wheel based on the present location of the bird.

At an early iteration, the value of $D(t)$ is closer to one for searching and exploring a new space. Based on its location and randomly selected neighbor, the red kite explores novel spaces in the movement depending on the separate module. In addition, the social component leads to global optima. The coefficient $D(t)$ decreases to accomplish a balance between the exploitation and exploration stages as the process moves from the initial to the next rounds. At the last iteration, this coefficient becomes 0 and the exploit searching for the optimum solutions amongst the better solution attained. The ROA has a high convergence level, few control parameters and ease of execution.

The RKO approach develops an FF to make effective classifier results. It expresses an optimistic integer to denote the good solution of candidate results. Throughout this case, the decrease in classifier errors can be assumed as FF, as represented in Eq. (8).

$$fitness(x_i) = ClassifierErrorRate(x_i) = \frac{No.of\ misclassified\ samples}{Total\ no.of\ samples} \times 100 \quad (8)$$

D. Image Classification Using DCAE

The Dilation Convolutional Autoencoder (DCAE) architecture can be used for classifying COVID-19 cases. A Convolutional Autoencoder (CAE) is a type of self-supervised learning model that learns to encode and decode data using convolution operations, aiming to reconstruct the original input. CAEs are widely used for tasks like anomaly detection, data compression, and noise removal [29].

A typical CAE has two parts: an encoder and a decoder. The encoder uses convolution and pooling layers to extract features and reduce data size, while the decoder uses upsampling and deconvolution layers to rebuild the original input. However, pooling layers can sometimes cause loss of important features because they reduce data size too much and limit the detail captured.

To solve this, the DCAE replaces the pooling layers with dilated convolutions. This helps compress the data while preserving important information, making the model more effective for medical image classification.

The obtained signal covariance matrix with no reflected angle is represented by R'_x, only have the elevation and azimuth angles of non-lower elevation traget and the azimuth and direct angles of the lower elevation traget; the real and imaginary equation of the signal can be denoted $Re(*)$ and $Im(*)$, correspondingly. The encoder Eq. (9) and decoder Eq. (10) processes are given as follows,

$$Encoding: y = f_e(R_x), \quad (9)$$

$$Decoding: R_{\dot{x}} = f_d(y), \quad (10)$$

where the received signal covariance matrix with reflected angle is referred to as R_x, which is the original signal covariance matrix. Further, the proposed dilated CAE Eq. (11) can be described as follows:

$$R'_x = f_d\big(f_e(R_x)\big), \quad (11)$$

This implies that mapping between covariance matrix with and without reflection angle can be accomplished as follows:

$$h^n = f(R.w^n + b^n), \quad (12)$$

In Eq. (12), R illustrates the input 3D matrix, 3D convolution kernel has been named as w, and the bias is denoted as b^n whose number is n; and the activation function can be denoted as $f(*)$. The decoder process carries out the deconvolution function that is almost identical to the convolutional process. The two convolution layers in the blue box can be typical convolution processes with padding that targets to preserve the boundary feature. The binary cross-entropy process is a loss function of DCAE (Eq. (13)) as follows:

$$bce = -\sum_{i=1}^{N}\sum_{j=1}^{N}\big(r_{ij}\log(r'_{ij}) + (1 - r_{ij})\log(1 - r'_{ij})\big) \quad (13)$$

IV. Results and Discussion

In this study, the COVID-19 detection accomplishment of the BRKODL-COVIDC method is examined by employing the CXR dataset [30]. The dataset description is given in Table 1.

Table 1. Database details

Classes	Image Numbers
ARDS	15
COVID-19	220
No Finding	27
Pneumocystis	15
SARS	11
Streptococcus	17
Overall Images	305

Fig. 3 portrays the confusion matrices formed by BRKODL-COVIDC model at 80:20 and 70:30 of the TRAP/TESP. The investigational output pointed out the efficient recognition of the overall 6 classes.

The COVID-19 classifying outputs of the BRKODL-COVIDC model under 80:20 of TRAP/TESP are illustrated in Table 2 and Fig. 4. The investigational outputs emphasized that the BRKODL-COVIDC model precisely classified different classes. On 80% of the TRAP, the BRKODL-COVIDC model obtains an average $accu_y$ of 99.59%, precision of 99.72%, sensitivity of 96.53%, specificity of 99.28%, and F-score of 97.99%. Similarly, with 20% of the TESP, the BRKODL-COVIDC model increases average accuracy of 98.91%, precision of 94.08%, sensitivity of 94.44%, specificity of 98.68%, and F-score of 93.15%, respectively.

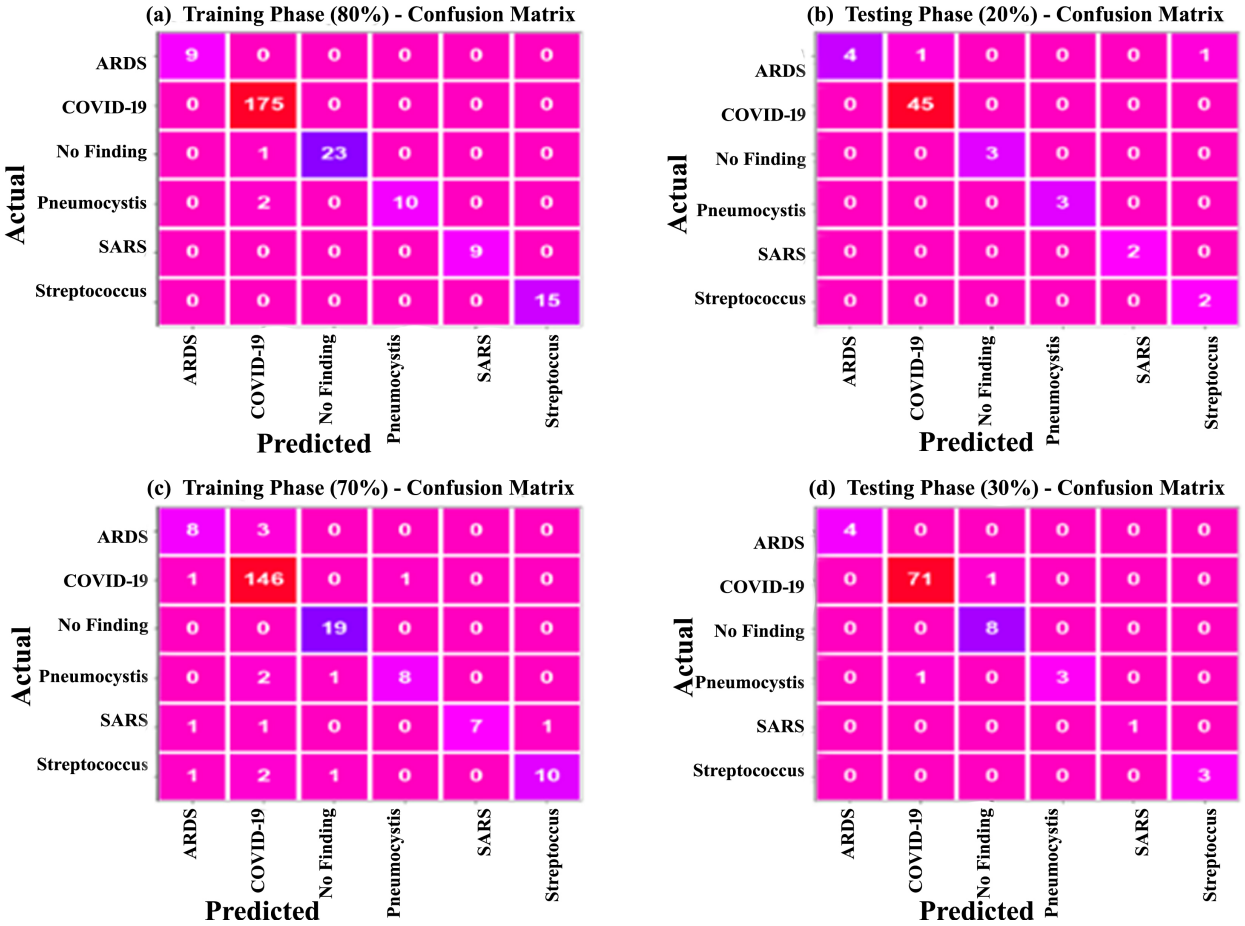

Fig. 3. Confusion matrices of (a–c) 80:70 TRAP and (b–d) 20:30 TESP.

Table 2. COVID-19 classifier outcome of BRKODL-COVIDC approach at 80:20 of TRAP/TESP

Class	Disease	$Accu_y$ /%	$Prec_n$ /%	$Sens_y$ /%	$Spec_y$ /%	F_{score} /%
TRAP (80%)	ARDS	100.00	100.00	100.00	100.00	100.00
	COVID-19	98.77	98.31	100.00	95.65	99.15
	No Finding	99.59	100.00	95.83	100.00	97.87
	Pneumocystis	99.18	100.00	83.33	100.00	90.91
	SARS	100.00	100.00	100.00	100.00	100.00
	Streptococcus	100.00	100.00	100.00	100.00	100.00
	Average	**99.59**	**99.72**	**96.53**	**99.28**	**97.99**
TESP (20%)	ARDS	96.72	100.00	66.67	100.00	80.00
	COVID-19	98.36	97.83	100.00	93.75	98.90
	No Finding	100.00	100.00	100.00	100.00	100.00
	Pneumocystis	100.00	100.00	100.00	100.00	100.00
	SARS	100.00	100.00	100.00	100.00	100.00
	Streptococcus	98.36	66.67	100.00	98.31	80.00
	Average	**98.91**	**94.08**	**94.44**	**98.68**	**93.15**

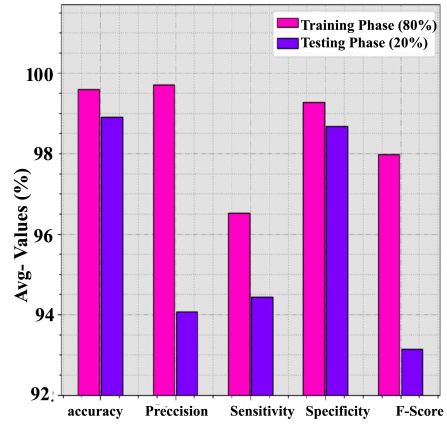

Fig. 4. Average of BRKODL-COVIDC method at 80:20 of TRAP/TESP.

The encoding and decoding were calculated with the help of Eqs. (9)–(11). The performance analysis of the proposed BRKODL-COVIDC methodology for COVID-19 classification, using a 70:30 split between training (TRAP) and testing (TESP) datasets, is presented in Table 3 and illustrated in Fig. 5. The simulation results confirm that the BRKODL-COVIDC model effectively distinguishes between multiple COVID-19 classes, demonstrating strong classification capability.

Table 3. COVID-19 classifier outcome of BRKODL-COVIDC model at 70:30 of TRAP/TESP

Class	Disease	$Accu_y$ /%	$Prec_n$ /%	$Sens_y$ /%	$Spec_y$ /%	F_{score} /%
TRAP (70%)	ARDS	97.18	72.73	72.73	98.51	72.73
	COVID-19	95.31	94.81	98.65	87.69	96.69
	No Finding	99.06	90.48	100.00	98.97	95.00
	Pneumocystis	98.12	88.89	72.73	99.50	80.00
	SARS	98.59	100.00	70.00	100.00	82.35
	Streptococcus	97.65	90.91	71.43	99.50	80.00
	Average	97.65	89.63	80.92	97.36	84.46
TESP (30%)	ARDS	100.00	100.00	100.00	100.00	100.00
	COVID-19	97.83	98.61	98.61	95.00	98.61
	No Finding	98.91	88.89	100.00	98.81	94.12
	Pneumocystis	98.91	100.00	75.00	100.00	85.71
	SARS	100.00	100.00	100.00	100.00	100.00
	Streptococcus	100.00	100.00	100.00	100.00	100.00
	Average	99.28	97.92	95.60	98.97	96.41

When trained on 70% of the data (TRAP), the model achieved an average accuracy of 97.65%, precision of 89.63%, recall of 80.92%, specificity of 97.36%, and F1-score of 84.46%. These values indicate that the model

performs consistently well across different performance metrics, particularly in recognizing positive and negative cases with high specificity.

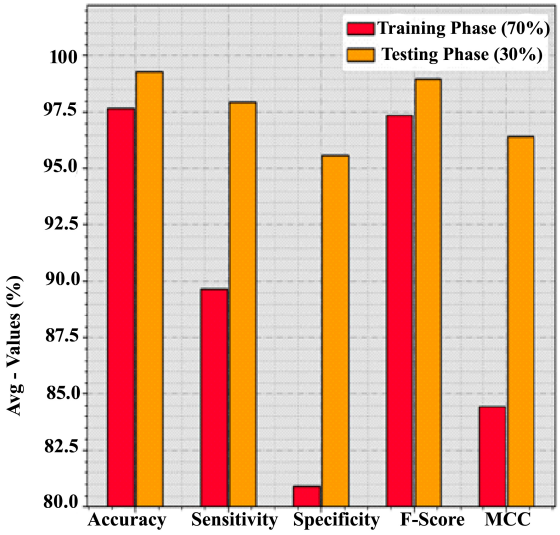

Fig. 5. Average of BRKODL-COVIDC model at 70:30 of TRAP/TESP.

Furthermore, when evaluated on the remaining 30% of the data (TESP), the BRKODL-COVIDC model delivered even better performance, achieving an average accuracy of 99.28%, precision of 97.92%, recall of 95.60%, specificity of 98.97%, and F1-score of 96.41%. These results demonstrate the robustness and generalization capability of the model, confirming its suitability for reliable COVID-19 classification in practical scenarios.

To evaluate the accomplishment of the BRKODL-COVIDC technique with 80:20 of TRAP/TESP, Training and Testing accuracy curves are determined, as portrayed in Fig. 6. The TRA and TES accuracy curves display the performance of BRKODL-COVIDC technique over several epochs. The figure exhibits the capability of the learning tasks and generalized abilities of the BRKODL-COVIDC technique. As the epoch rises, it is perceived that the TRA and TES accuracy curves attain improvement. It is detected that the BRKODL-COVIDC technique obtains amended testing accuracy for identifying the patterns in the TRA and TES data.

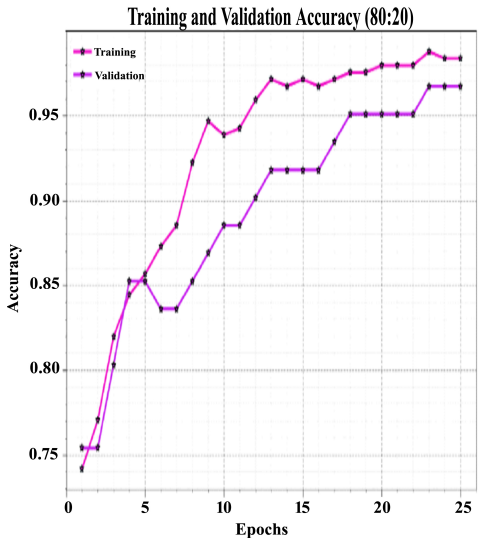

Fig. 6. $Accu_y$ curve of BRKODL-COVIDC model at 80:20 of TRAP/TESP.

Fig. 7 demonstrated the complete loss values of the TRA and TES of the BRKODL-COVIDC approach with 80:20 of TRAP/TESP over epochs. The TRA loss signified the loss reduces over epochs. Chiefly, the loss decreases as the model alters the weight to decline the forecast error on the TRA and /TES data. The loss curves exhibit the level to which the model is fitting the TRA data. It is seen that the TRA and TES losses are slowly minimized, and it is defined that the modified BRKODL-COVIDC method effectively learns the patterns shown in the TR and TS data. The BRKODL-COVIDC method modified the parameters to reduce the discrepancies between the forecast and the actual TRA label.

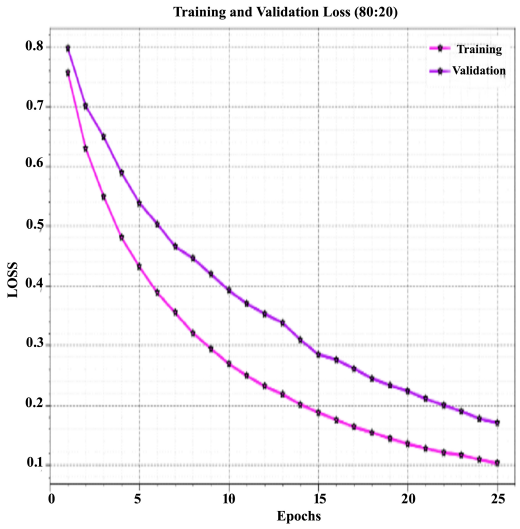

Fig. 7. Loss curve of BRKODL-COVIDC method at 80:20 of TRAP/TESP.

The Plotting accuracy alongside recall illustrates the Precision-Recall (PR) accomplishment of the BRKODL-COVIDC method with an 80:20 TRAP/TESP ratio, as presented in Fig. 8. The investigational outputs showed that the BRKODL-COVIDC method acquires enhanced PR with each 6 classes. The figure indicates that the technique learns to identify five discrete classes. The BRKODL-COVIDC method attains augmented outputs in the detection of positive instances with decreased false positives.

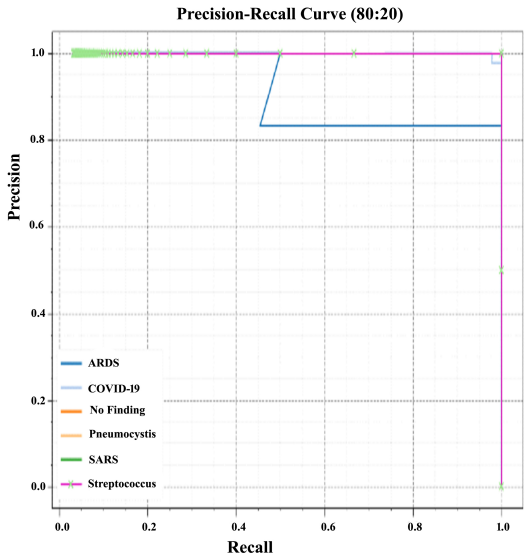

Fig. 8. PR curve of BRKODL-COVIDC method at 80:20 of TRAP/TESP.

The ROC study shown by the BRKODL-COVIDC system, which uses an 80:20 ratio of TRAP/TESP, is displayed in Fig. 9 and can tell apart the 5 classes. The figure provided valuable details about the trade-off between the True Positive Rate (TPR) and False Positive Rate (FPR) across various classification thresholds and different epoch counts. It precisely portrays the anticipated accomplishment of the BRKODL-COVIDC system through the identification of six diverse classes.

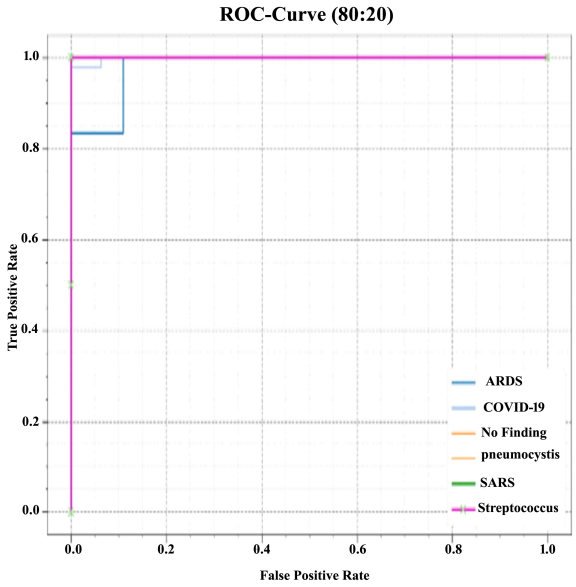

Fig. 9. ROC curve of BRKODL-COVIDC method at 80:20 of TRAP/TESP.

The COVID-19 classification results using the proposed BRKODL-COVIDC method, along with other recent deep learning models, are shown in Table 4 and Fig. 10. The experimental results show that the DLS-SCD method performs poorly. In comparison, methods like InceptionV3, ResNet-50, VGG16, and AD-TLCNN perform slightly better. The SCODL-DDC method achieves relatively good results. However, the BRKODL-COVIDC method outperforms all others, achieving an accuracy of 99.59%, precision of 96.53%, recall of 99.28%, and F1-score of 97.99%. These results clearly demonstrate that BRKODL-COVIDC delivers superior performance in COVID-19 classification.

Table 4. Relative output of BRKODL-COVIDC approach with recent DL models

Methods	$Accu_y$/%	$Sens_y$/%	$Spec_y$/%	F_{score}/%
BRKODL-COVIDC	99.59	96.53	99.28	97.99
SCODL-DDC	99.45	95.65	99.11	97.27
InceptionV3	97.65	94.26	97.68	90.43
ResNet50	97.08	88.17	97.85	84.07
VGG16	96.59	86.57	97.80	83.26
DLS-SCD	86.44	86.21	86.66	86.01
AD-TLCNN	95.07	95.46	97.18	92.33

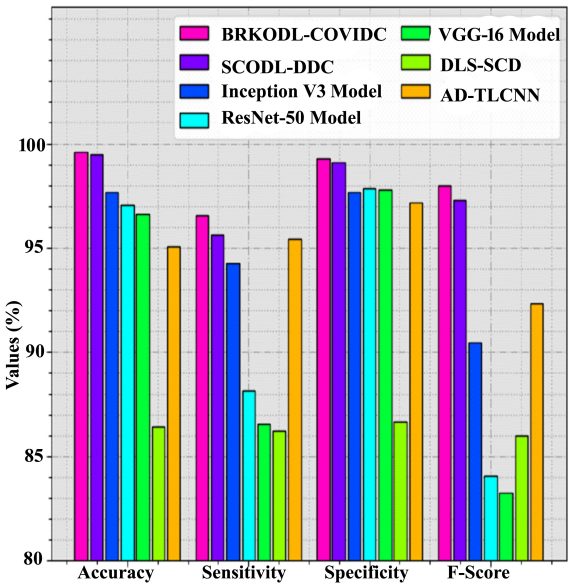

Fig. 10. Comparative outcome of BRKODL-COVIDC method with current DL methods.

V. Conclusion

This study paper proposes the BRKODL-COVIDC approach, an automated model for COVID-19 recognition and classification on CXR images. The aim of the BRKODL-COVIDC approach is to detect and identify the models. The presented BRKODL-COVIDC technique utilizes four main functions: BF-based pre-processing, DenseNet121 feature extractor, RKO-based hyperparameter tuning, and DCAE-based classification. In this work, the complex patterns and features in the images can be derived from the DenseNet121 model. For optimal hyperparameter selection of the DL methods, the RKO model can be applied in this study. Finally, the BRKODL-COVIDC technique employs the DCAE model and is utilized for classification purposes. The simulation outcomes of the BRKODL-COVIDC model are experimented on with a standard dataset. The simulation outputs described the improved accomplishment of the BRKODL-COVIDC model for the COVID-19 detection process. Thus, the study offers solutions for sustainable health care that aim to maintain a sustainable health environment for public health challenges and contribute to the national priorities of RDI.

Conflict of Interest

The authors declare no conflict of interest.

Author Contributions

Conceptualization, M.A.A., S.A., S.N.M., P.K., B.B.D.; methodology, M.A.A. S.A., S.N.M., P.K., B.B.D.; software, M.A.A. S.A., S.N.M., P.K., B.B.D.; validation, M.A.A. S.A., S.N.M., P.K., B.B.D., Q.M.,; formal analysis, S.A., S.N.M., P.K., B.B.D.; investigation, M.A.A. S.A., S.N.M., P.K., B.B.D., Q.M.; resources, S.A., S.N.M., P.K., B.B.D.; data curation, M.A.A.; writing original draft preparation, M.A.A.; writing review and editing, M.A.A. S.A., S.N.M., P.K., B.B.D.; visualization, M.A.A. S.A., S.N.M., P.K., B.B.D., Q.M.; supervision, S.A., S.N.M., P.K., B.B.D.; project administration, M.A.A., S.A., S.N.M., P.K., B.B.D.; funding

acquisition, S.A. All authors have read and agreed to the published version of the manuscript.

FUNDING

This research was funded by Prince Sattam bin Abdulaziz University, Al-Kharj, Saudi Arabia, through project grant number (PSAU-2024/01/31379).

ACKNOWLEDGEMENT

The authors extend their appreciation to Prince Sattam bin Abdulaziz University for funding this research work through the project number (PSAU-2024/01/31379).

REFERENCES

[1] M. E. Sahin, H. Ulutas, E. Yuce *et al.*, "Detection and classification of COVID-19 by using faster R-CNN and mask R-CNN on CT images," *Neural Computing and Applications*, vol. 35, no. 18, pp. 13597–13611, 2023.

[2] Ç. Oğuz and M. Yağanoğlu, "Detection of COVID-19 using deep learning techniques and classification methods," *Information Processing & Management*, vol. 59, no. 5, 103025, 2022.

[3] E. Hussain, M. Hasan, M. A. Rahman *et al.*, "CoroDet: A deep learning-based classification for COVID-19 detection using chest X-ray images," *Chaos, Solitons & Fractals*, vol. 142, 110495, 2021.

[4] H. Zhu, Z. Zhu, S. Wang *et al.*, "CovC-ReDRNet: A deep learning model for COVID-19 classification," *Machine Learning and Knowledge Extraction*, vol. 5, no. 3, pp. 684–712, 2023.

[5] W. A. Shehri, J. Almalki, R. Mehmood *et al.*, "A novel COVID-19 detection technique using deep learning based approaches," *Sustainability*, vol. 14, no. 19, 12222, 2022.

[6] A. I. Khan, J. L. Shah, and M. M. Bhat, "CoroNet: A deep neural network for detection and diagnosis of COVID-19 from chest X-ray images," *Computer Methods and Programs in Biomedicine*, vol. 196, 105581, 2020.

[7] N. Agarwal, S. N. Mohanty, S. Sankhwar *et al.*, "A novel model to predict the effects of enhanced students' computer interaction on their health in COVID-19 pandemics," *New Generation Computing*, vol. 41, no. 3, pp. 635–668, 2023. https://doi.org/10.1007/s00354-023-00224-3

[8] V. Rastogi and A. K. Jain, "Detection and classification of COVID-19 disease using SWHO-based deep neural network classifier," *Computer Methods in Biomechanics and Biomedical Engineering: Imaging & Visualization*, vol. 11, no. 6, pp. 2183–2195, 2023.

[9] S. K. Satapathy, S. Saravanan, S. Mishra *et al.*, "A comparative analysis of multidiemnsional COVID-19 poverty determinants: An observational machine learning approach," *New Generation Computing*, vol. 41, no. 1, pp. 155–184, 2023. https://doi.org/10.1007/s00354-023-00203-8

[10] M. A. Khan, M. Azhar, K. Ibrar *et al.*, "COVID-19 classification from chest X-ray images: A framework of deep explainable artificial intelligence," *Computational Intelligence and Neuroscience*, vol. no. 1, 2022.

[11] G. S. Chakraborty, S. Batra, A. Singh *et al.*, "A novel deep learning-based classification framework for COVID-19 assisted with weighted average ensemble modeling," *Diagnostics*, vol. 13, no. 10, 1806, 2023.

[12] S. Kumar, S. K. Gupta, V. Kumar *et al.*, "Ensemble multimodal deep learning for early diagnosis and accurate classification of COVID-19," *Computers and Electrical Engineering*, vol. 103, 108396, 2022.

[13] S. Sah, B. Surendiran, R. Dhanalakshmi *et al.*, "Forecasting COVID-19 pandemic using prophet, ARIMA, and hybrid stacked LSTM-GRU models in India," *Computational and Mathematical Methods in Medicine*, vol. 2022, no. 1, 2022. doi:10.1155/2022/1556025

[14] K. Gupta and V. Bajaj, "Deep learning models-based CT-scan image classification for automated screening of COVID-19," *Biomedical Signal Processing and Control*, vol. 80, 104268, 2023.

[15] R. F. Mansour, J. Escorcia-Gutierrez, M. Gamarra *et al.*, "Unsupervised deep learning-based variational autoencoder model for COVID-19 diagnosis and classification," *Pattern Recognition Letters*, vol. 151, pp. 267–274, 2021.

[16] S. Sakib, T. Tazrin, M. M. Fouda *et al.*, "DL-CRC: Deep learning-based chest radiograph classification for COVID-19 detection: A novel approach," *IEEE Access*, vol. 8, pp.171575–171589, 2020.

[17] D. Shome, T. Kar, S. N. Mohanty *et al.*, "COVID-Transformer: Interpretable COVID-19 detection using vision transformer for healthcare," *International Journal of Environmental Research and Public Health*, vol. 18, no. 21, 11086, 2021. https://doi.org/10.3390/ijerph182111086

[18] R. T. Subhalakshmi, S. A. A. Balamurugan, and S. Sasikala, "Deep learning-based fusion model for COVID-19 diagnosis and classification using computed tomography images," *Concurrent Engineering*, vol. 30, no. 1, pp. 116–127, 2022.

[19] K. Shankar, S. N. Mohanty, K. Yadav *et al.*, "Automated COVID-19 diagnosis and classification using convolutional neural network with fusion based feature extraction model," *Cognitive Neurodynamics*, vol. 17, pp. 1–14, 2023. doi:10.1007/s11571-021-09712-y

[20] A. Shanthi and S. Koppu, "Remora namib beetle optimization enabled deep learning for severity of COVID-19 lung infection identification and classification using CT images," *Sensors*, vol. 23, no. 11, 5316, 2023.

[21] S. Dash, S. Chakravati, S. N. Mohanty *et al.*, "A deep learning method to forecast COVID-19 outbreak," *New Generation Computing*, vol. 39, pp. 515–539, 2021. doi: 10.1007/s00354-021-00129-z

[22] D. N. Le, V. S. Parvathy, D. Gupta *et al.*, "IoT-enabled depthwise separable convolution neural network with deep support vector machine for COVID-19 diagnosis and classification," *International Journal of Machine Learning and Cybernetics*, vol. 12, no. 11, pp. 3235–3248, 2021.

[23] S. Satpathy, M. Mangala, N. Sharma *et al.*, "Predicting mortality rate and associated risks in COVID-19 patients," *Spatial Information Research*, vol. 29, pp. 455–464, 2021. doi: 10.1007/s41324-021-00379-5

[24] N. Sharma, L. Saba, N. N. Khanna *et al.*, "Segmentation-based classification deep learning model embedded with explainable AI for COVID-19 detection in chest X-ray scans," *Diagnostics*, vol. 12, no. 9, 2132, 2022.

[25] T. Althaqafi, A. S. A. M. Al-Ghamdi and M. Ragab, "Artificial intelligence based COVID-19 detection and classification model on chest X-ray images," *Healthcare*, vol. 11, no. 9, 1204, 2023.

[26] J. Ai, R. Liu, B. Tang *et al.*, "A refined bilateral filtering algorithm based on adaptively-trimmed statistics for speckle reduction in SAR imagery," *IEEE Access*, vol. 7, pp. 103443–103455, 2019.

[27] T. Chauhan, H. Palivela, and S. Tiwari, "Optimization and fine-tuning of DenseNet model for classification of COVID-19 cases in medical imaging," *International Journal of Information Management Data Insights*, vol. 1, no. 2, 100020, 2021. doi: 10.1016/j.jjimei.2021.100020

[28] S. M. Alshareef and A. Fathy, "Efficient red kite optimization algorithm for integrating the renewable sources and electric vehicle fast charging stations in radial distribution networks," *Mathematics*, vol. 11, no. 15, 3305, 2023.

[29] G. Hu, F. Zhao, and B. Liu, "Estimation of the two-dimensional direction of arrival for low-elevation and non-low-elevation targets based on dilated convolutional networks," *Remote Sensing*, vol. 15, no. 12, 3117, 2023.

[30] COVID-19 dataset. *GitHub.* [Online]. Available: https://github.com/ieee8023/covid-chestxray-dataset